

OPEN ACCESS

## Impact of Testing Method on Safety Assessment of Aged Li-Ion Cells: Part II – Aged Cells Without Li Plating

To cite this article: Yuliya Preger *et al* 2025 *J. Electrochem. Soc.* **172** 080503

View the [article online](#) for updates and enhancements.

### You may also like

- [Revealing the Unique Influential Mechanism of Parallel-Connected Lithium-Ion Cells Based on Current Distribution: The Vectorial Effect among Cell-to-Cell Parameters](#)  
Shuyu Yuan, Shiyi Fu, Kun He et al.
- [Microstructure Scale Lithium-Ion Battery Modeling, Part IV: The Representativity of Microstructure Parameters and Electrochemical Response](#)  
Francois L. E. Usseglio-Viretta, Andrew M. Colclasure, Jeffery Allen et al.
- [Tuning of Cathode Compositions to Boost Performance of MoS<sub>2</sub>-Based Hybrid Zn-air Batteries using PVA-CMC Gel Polymer Electrolytes](#)  
Vivek Kumar, Deepika Choudhary, Akshidha Singla et al.

## Your Lab in a Box!

The PAT-Tester-i-16 Multi-Channel Potentiostat for Battery Material Testing!

- ✓ **All-in-One Solution with Integrated Temperature Chamber (+10 to +80 °C)!**  
No additional devices are required to measure at a stable ambient temperature.
- ✓ **Fully Featured Multi-Channel Potentiostat / Galvanostat / EIS!**  
Up to 16 independent battery test channels, no multiplexing.
- ✓ **Ideally Suited for High-Precision Coulometry!**  
Measure with excellent accuracy and signal-to-noise ratio.
- ✓ **Small Footprint, Easy to Setup and Operate!**  
Cableless connection of 3-electrode battery test cells. Powerful EL-Software included.

**EL-CELL®**  
electrochemical test equipment



Learn more on our product website:



Download the data sheet (PDF):



Or contact us directly:

+49 40 79012-734

[sales@el-cell.com](mailto:sales@el-cell.com)

[www.el-cell.com](http://www.el-cell.com)



# Impact of Testing Method on Safety Assessment of Aged Li-Ion Cells: Part II – Aged Cells Without Li Plating

Yuliya Preger,<sup>1,\*,z</sup> Max Feinauer,<sup>2,=</sup> Loraine Torres-Castro,<sup>3,\*</sup> Christin Hogrefe,<sup>2</sup> Lucas Gray,<sup>3</sup> Gabriela Gerosa,<sup>2</sup> Jill Langendorf,<sup>3</sup> Samuel Häfele,<sup>2</sup> Reed M. Wittman,<sup>1,\*</sup> Michael Wörz,<sup>2</sup> Chaz Rich,<sup>3</sup> Olaf Böse,<sup>2</sup> Markus Hölzle,<sup>2</sup> Nathan Brenner Johnson,<sup>3,\*</sup> Margret Wohlfahrt-Mehrens,<sup>2,4,\*</sup> and Thomas Waldmann<sup>2,4,5,\*</sup>

<sup>1</sup>Energy Storage Tech & Systems, Sandia National Laboratories, Albuquerque, New Mexico, 87185, United States of America

<sup>2</sup>Zentrum für Sonnenenergie- und Wasserstoff-Forschung (ZSW), 89081 Ulm, Germany

<sup>3</sup>Power Sources R&D, Sandia National Laboratories, Albuquerque, New Mexico, 87185, United States of America

<sup>4</sup>Helmholtz Institute Ulm for Electrochemical Energy Storage (HIU), 89081 Ulm, Germany

<sup>5</sup>Institute of Surface Chemistry and Catalysis, Ulm University, 89069 Ulm, Germany

Understanding the safety profile of aged Li-ion batteries is essential for developing effective battery management and hazard mitigation strategies. However, most safety assessments have focused on fresh batteries, with just a few calorimetry studies on aged batteries with metal oxide positive electrodes. This study provides a broad assessment of commercial 18650-type Li-ion batteries with NCA, NMC, and LFP positive electrodes, both uncycled and aged under conditions that promoted solid electrolyte interphase (SEI) growth as the dominant degradation mechanism. The cells underwent mechanical (nail penetration, crush), electrical (overcharge, overdischarge), and thermal (accelerating rate calorimetry) abuse tests. Safety was rated on general characteristics such as mass loss, maximum temperature, and EUCAR (European Council for Automotive R&D) hazard level, as well as characteristics specific to individual abuse tests. Generally, aged cells with SEI growth exhibited similar or improved safety compared to uncycled cells, contrasting with our previous findings on NCA cells with Li plating as the dominant aging mechanism (Part I of this series). Yet, some tests and characteristics indicated reduced aged cell safety, such as earlier triggering of mechanical failure. These results emphasize the need to examine aged battery safety across diverse empirical techniques, degradation modes, and chemistries.

© 2025 The Author(s). Published on behalf of The Electrochemical Society by IOP Publishing Limited. This is an open access article distributed under the terms of the Creative Commons Attribution 4.0 License (CC BY, <https://creativecommons.org/licenses/by/4.0/>), which permits unrestricted reuse of the work in any medium, provided the original work is properly cited. [DOI: 10.1149/1945-7111/adeed0]



Manuscript submitted March 20, 2025; revised manuscript received June 18, 2025. Published August 1, 2025.

Supplementary material for this article is available [online](#)

Li-ion batteries (LIBs) are attractive for a variety of applications, from consumer electronics to grid energy storage, but their failure can have severe consequences. Diverse electrical, mechanical, and thermal abuse conditions can prompt thermal runaway (TR), a phenomenon wherein uncontrollable exothermic reactions inside a cell exponentially increase its temperature, causing the cell to catch fire or explode.<sup>1–4</sup> Quantifying the conditions at which TR is triggered and the magnitude of failure is essential for designing appropriate detection and mitigation approaches.<sup>5–9</sup>

Most research on battery safety has focused on fresh cells (uncycled), potentially under the assumption that aged cells will exhibit similar or less severe abuse responses due to their reduced capacity.<sup>10</sup> However, aging alters material properties and electrochemical performance through mechanisms such as solid electrolyte interphase (SEI) growth, Li plating, gas generation, and electrode degradation.<sup>11–13</sup> Both SEI growth and Li plating consume cyclable Li, also known as loss of lithium inventory (LLI).<sup>14,15</sup> These changes can influence how a cell responds to abuse, potentially introducing new safety risks or mitigating others. As LIBs are considered for second-life applications in stationary energy storage systems, evaluating the safety of aged cells has become more important than ever.

Recent studies have investigated the difference in the abuse response of uncycled and aged Li-ion cells using accelerating rate calorimetry (ARC).<sup>8,16–30</sup> In these tests, batteries with primarily metal oxide positive electrodes were heated at a constant rate to a set temperature or failure. Critical battery safety characteristics included the onset temperatures of self-heating ( $T_{SH}$ ) and thermal runaway ( $T_{TR}$ ), and the peak temperature ( $T_{max}$ ). Variations in onset

temperatures for similar chemistries are related to the kinetics of decomposition reactions and the peak temperature is generally correlated to the stored energy in the cell.<sup>24</sup> Both are important for evaluating the relative safety of aged cells with respect to new cells of the same type. A cell is considered safer if its onset temperatures are higher (delayed TR) or peak temperature is lower (lower total heat release) when compared to another cell design. Li plating on the negative electrode consistently lowered onset temperatures by up to 50 °C, due to exothermic reaction of the Li with the electrolyte.<sup>17,25–28,31</sup> For conditions where cells only exhibited Li loss through SEI growth or general active material loss, onset temperatures were similar to those of fresh cells or even higher.<sup>17,21,26</sup> A comprehensive assessment of most public calorimetry results of aged LIBs is given in a previous review.<sup>24</sup> This review highlighted several relevant questions on the safety of aged LIBs, including: (1) how do cells respond to *different abuse techniques* when SEI growth is the primary aging mechanism, and (2) how do trends vary across *different chemistries* (especially LFP positive electrodes).<sup>32–43</sup>

In this work, we evaluate the abuse response of aged cells of three different positive electrode chemistries (NCA, NMC, and LFP) across multiple experimental safety test methods (overcharge, overdischarge, ARC, nail penetration, and crush), with SEI growth as the dominant degradation mechanism. We assess safety characteristics specific to each abuse technique (e.g., time to current interrupt device (CID) activation for overcharge, as well as displacement and load for nail penetration). We also consider characteristics applicable to all safety tests: maximum temperature, mass loss, and EUCAR (European Council for Automotive R&D) hazard rating. This publication is the second of two papers focusing on the safety assessment of Li-ion cells with different aging mechanisms. Our previous assessment of NCA cells with Li plating as the dominant degradation mechanism showed that the aged cells were less safe

<sup>\*</sup>Equal Contribution.

<sup>\*</sup>Electrochemical Society Member.

<sup>z</sup>E-mail: [ypreger@sandia.gov](mailto:ypreger@sandia.gov); [thomas.waldmann@zsw-bw.de](mailto:thomas.waldmann@zsw-bw.de)

across all safety characteristics.<sup>31</sup> Here, we found that uncycled and aged cells with SEI growth generally demonstrate a similar magnitude of TR in response to abuse. However, in some cases, the sensitivity to triggering TR changed. Specifically, aged cells tolerated more overcharge and overdischarge prior to failure, but less mechanical insult during nail penetration. These results emphasize the need to report aged battery safety across diverse safety techniques and characteristics.

## Experimental

**Cell details.**—Table I notes the specifications of the commercial 18650 cells evaluated in this work, including the manufacturer-recommended operating limits. These represent popular cathode materials that are also more likely to be utilized in second-life battery applications. All experiments with NCA cells were carried out at ZSW (Zentrum für Sonnenenergie- und Wasserstoff-Forschung Baden-Württemberg) and all the experiments with NMC and LFP cells were carried out at SNL (Sandia National Labs).

**Aging conditions.**—This study used NMC and LFP cells aged in a previous study.<sup>44</sup> Briefly, cycle aging was carried out using an Arbin SCTS and an Arbin high-precision (Model: LBT21084) multi-channel battery testing system, and cells were placed in SPX Tenney Model T10C-1.5 environmental chambers. The cells were aged under a variety of temperatures (15, 25, or 35 °C), discharge C-rates (0.5C, 1C, 2C, or 3C), and state-of-charge windows (40%–60%, 20%–80%, or 0%–100%), as shown in Table S1. A number of cells which had reached the desired remaining capacity values (approximately 80%, 70%, or 40%) were selected for abuse testing in the present study. The lack of Li plating in NMC cells aged under comparable conditions was confirmed by visual inspection and scanning electron microscopy (SEM).<sup>45</sup> The lack of Li plating in the LFP cells was assessed by electrochemical experiments (Arrhenius plots of the capacity-based aging rates and discharge voltage profiles). The precise cycle aging conditions for the LFP and NMC cells used in this study are given in the Supporting Information (Table S2) and their aging trends are shown in Fig. S1. In the meantime, uncycled cells were stored fully discharged. Prior to the abuse tests, the capacities of the uncycled cells were tested to verify that they were still close to the nominal capacity.

NCA cells were cycle-aged with BaSyTec CTS systems in Binder ovens at 45 °C ambient temperature. Cycle aging of the cells was performed with 0.5C charging rate (constant current-constant voltage, 0.05C cut-off current) and 0.5C discharging rate. The C-rate was based on the nominal capacity of the cells. The aging was stopped when the batteries reached a remaining discharge capacity  $\leq 81\%$  relative to the first cycle discharge capacity. All cells reached  $\sim 80\%$  remaining discharge capacity after  $294 \pm 42$

cycles. The full aging trends of the cells are shown in Fig. S2. Under these aging conditions, the NCA cells did not show lithium plating in post-mortem analysis (visual inspection, SEM, and glow discharge optical emission spectrometry depth profiling) and electrochemical experiments (Arrhenius plots of the capacity-based aging rates and discharge voltage profiles).<sup>31</sup>

The above cycling conditions may be different from the duty profiles that batteries are subjected to in the field. However, this study is intended to investigate the safety impacts of a specific degradation mechanism (SEI formation), that is common to many duty profiles.

**Safety testing protocols.**—Table II summarizes the safety hazard tests applied to the uncycled and aged cells, including overcharge, overdischarge, ARC, nail penetration, and crush. Overcharge, overdischarge, nail penetration, and ARC tests were performed independently on uncycled and aged cells. Crush was performed after the initial overcharge and overdischarge tests for safe disposal. The cells were tested using these independent safety testing methods to understand the impact of testing method on safety assessment; for example—if a cell appears safer according to certain safety characteristics in one test, but less safe according to safety characteristics in another test. Some safety tests were not applied to all cells based on equipment availability. The NCA cell experiments were conducted in triplicate to investigate the reproducibility of different abuse techniques. There were insufficient NMC and LFP cell quantities for replicates. All cells were charged to 100% SOC (state-of-charge) prior to the safety test, representing a worst-case failure scenario.

**Overcharge.**—A cell tester (Digatron UBT 150–020–3 RE) was used to perform the overcharge abuse tests on NCA cells. Temperature sensors were attached to the positive terminal, the negative terminal, and the surface of the cell housing. The LFP and NMC cells were overcharged using a power supply (Hewlett Packard PN# 6032 A, 0 to 50 A, 1000 W). Temperature sensors were attached to at least six locations on the cell: positive terminal, negative terminal, and various locations along the cell body. In all experiments, the fully charged cells were overcharged at 1C until 200% SOC (based on the nominal cell capacity) or an off-nominal event, whichever caused failure first.

**Overdischarge.**—Overdischarge experiments on NCA cells were carried out using the same equipment as the overcharge experiments. The LFP and NMC cells were overdischarged using a different power supply (Kepco PN#BOP 20–50MG, 0 to 50 A, 1000 W). For all three cell designs, fully charged cells were overdischarged at 1C until  $-150\%$  SOC (based on the nominal cell capacity) or failure, whichever happened first.

Table I. Overview of 18650 cell types and manufacturer specifications.

Cell <sup>a)</sup>	NCA	NMC	LFP
Positive Electrode	LiNi <sub>0.87</sub> Co <sub>0.10</sub> Al <sub>0.03</sub> O <sub>2</sub>	LiNi <sub>0.84</sub> Mn <sub>0.06</sub> Co <sub>0.10</sub> O <sub>2</sub>	LiFePO <sub>4</sub>
Negative Electrode	graphite	graphite + <5% silicon	graphite
Nominal Capacity (Ah)	3	3	1.1
Nominal Voltage (V)	3.65	3.6	3.3
Voltage Range (V)	2.5 to 4.2	2.0 to 4.2	2.0 to 3.6
Max Discharge Current (A)	6	20	30
Discharge Temperature Range (°C)	–20 to 55	–20 to 75	–30 to 60
Max Charge Current (A)	1.65	6	4
Charge Temperature Range (°C)	0 to 45	–5 to 50	–30 to 60
Nominal Mass (g)	48	47	39
Energy at 100% State-of-Charge (Wh)	10.95	10.8	3.63
Volumetric Energy Density (Wh/L)	661	652	219
1 kHz Impedance, Fully Charged (mΩ)	24.9	$\leq 20$	not reported

a) All cells had CIDs.

**Table II. Safety testing matrix for uncycled and aged cells.**

Cell name <sup>a)</sup>	Overcharge	Overdischarge	ARC	Nail penetration	Crush after over(dis)charge <sup>b)</sup>
NCA-uncycled	3	3	2	3	
NCA-aged-80%	3	3	2	3	
NMC-uncycled	1	1	1		1
NMC-aged-70%	1	1	1		2
NMC-aged-40%	1				1
LFP-uncycled	1	1	1		2
LFP-aged-80%	1	1	1		2

a) The number in the cell name refers to the percent remaining discharge capacity of the cell relative to its starting capacity. For brevity, this will also be referred to as the cell's state-of-health (SOH). b) Some cells were crushed after overcharge and overdischarge for safe disposal. Although this is not a standard safety test, the results were included here as they are relevant to general battery disposal and recycling operations.<sup>46</sup>

**Crush.**—Following overcharge and overdischarge, LFP and NMC cells were subject to mechanical crush to make them safe for disposal. Crush tests were conducted using a hydraulic press with a constant crush speed of  $0.1 \text{ mm s}^{-1}$ , applying force perpendicular to the largest surface of the cell. Tests were terminated upon 100% displacement or detection of thermal runaway. Surface temperatures were measured (only for LFP cells) using K-type thermocouples, and failure events were recorded in real-time.

**ARC.**—ARC experiments were conducted using Thermal Hazard Technology systems. While specific cell setups and test parameters varied slightly, the overall experimental procedure followed a consistent heat-wait-seek (HWS) procedure. The key setup details for each cell type are described in Table III and Figs. S3–5 show photos of the ARC systems.

The testing procedure for all cell types involved initiating the HWS program at a starting temperature of  $35^\circ\text{C}$  for NCA cells, and  $30^\circ\text{C}$  for LFP and NMC cells, with temperature increases in  $5^\circ\text{C}$  increments. After each increment, a wait period of 15 min (NCA) or 30 min (LFP and NMC) was followed by a  $\sim 10$  min seek period. If the self-heating rate (SHR) exceeded the exothermic sensitivity threshold of  $0.02^\circ\text{C min}^{-1}$ , the ARC automatically switched to exothermic mode, following the cell temperature.

**Nail penetration.**—Nail penetration tests were used to assess the safety characteristics of cells under mechanical insult resulting in an internal short circuit (ISC). Nail penetration tests were performed in a bunker (open system) on cells at 100% SOC. The force (max. 1 kN) and nail speed ( $0.1 \text{ mm s}^{-1}$ ) of the ceramic nail ( $\text{ZrO}_2$ ,  $\varnothing 3 \text{ mm}$ , tip angle =  $45^\circ$ ) were controlled by a linear drive. The nail was driven through the whole cell. Temperature sensors were attached to the positive terminal, the negative terminal, and the surface of the cell housing in the center of the cell.

## Results and Discussion

**Electrical safety tests.**—**Overcharge.**—Overcharge occurs when a cell is charged above the manufacturer's recommended upper cut-off voltage (end-of-charge voltage). This is a potential problem in battery packs with cell capacity imbalance, as well as packs with battery management or charging system failure. Previous studies of

fresh cells with metal oxide positive electrodes indicate that overcharge (transfer of excess Li from the positive to the negative electrode) can lead to structure destabilization, electrolyte degradation, and Li deposition on the negative electrode.<sup>47,48</sup> Here, overcharge abuse testing was conducted on 18650 cells with NCA, NMC, and LFP chemistries in both uncycled and aged states. All cells began at 100% SOC according to the manufacturer's cut-off voltage and were overcharged at a 1C rate (based on the nominal capacity of the cell type) until 200% SOC or until a failure, such as CID activation. CIDs, commonly found in 18650 cells, are intended to offer protection from overcharge by mechanically breaking the electrical circuit when triggered by excessive internal pressure.<sup>26</sup>

Figure 1 shows the voltage and temperature behavior for all three chemistries during overcharge, highlighting critical safety characteristics such as CID activation time and  $T_{\text{max}}$ . Visual failure behavior (e.g., electrolyte leakage, venting, fire) was also evaluated. Figure S6 shows the expanded voltage data during overcharge, including the voltage drop to 0 V which confirms the presence of a CID. Aged cells consistently exhibited longer CID activation times than uncycled cells. The CID activation time also aligned with  $T_{\text{max}}$  for all chemistries; once the CID is activated, current flow ceases, stopping ohmic heating. The observed activation times were:

- NCA cells - CID activation time increased from  $14.7 \pm 0.7 \text{ min}$  (uncycled) to  $19.0 \pm 1.1 \text{ min}$  (aged–80% SOH)
- NMC cells-CID activation time increased from 9.9 min (uncycled) to 11.3 min (aged–70% SOH) and 12.4 min (aged–40% SOH)
- LFP cells-CID activation time increased from 16.7 min (uncycled) to 24.3 min (aged–80% SOH)

Time served as the base metric of comparison, since SOC is a relative value and uncycled and aged cells have different starting discharge capacities. Nevertheless, SOC values at CID activation, calculated based on the nominal capacity of the uncycled cell, also show aged cells requiring a higher cumulative overcharge to activate the CID. The SOC values of CID activation were:

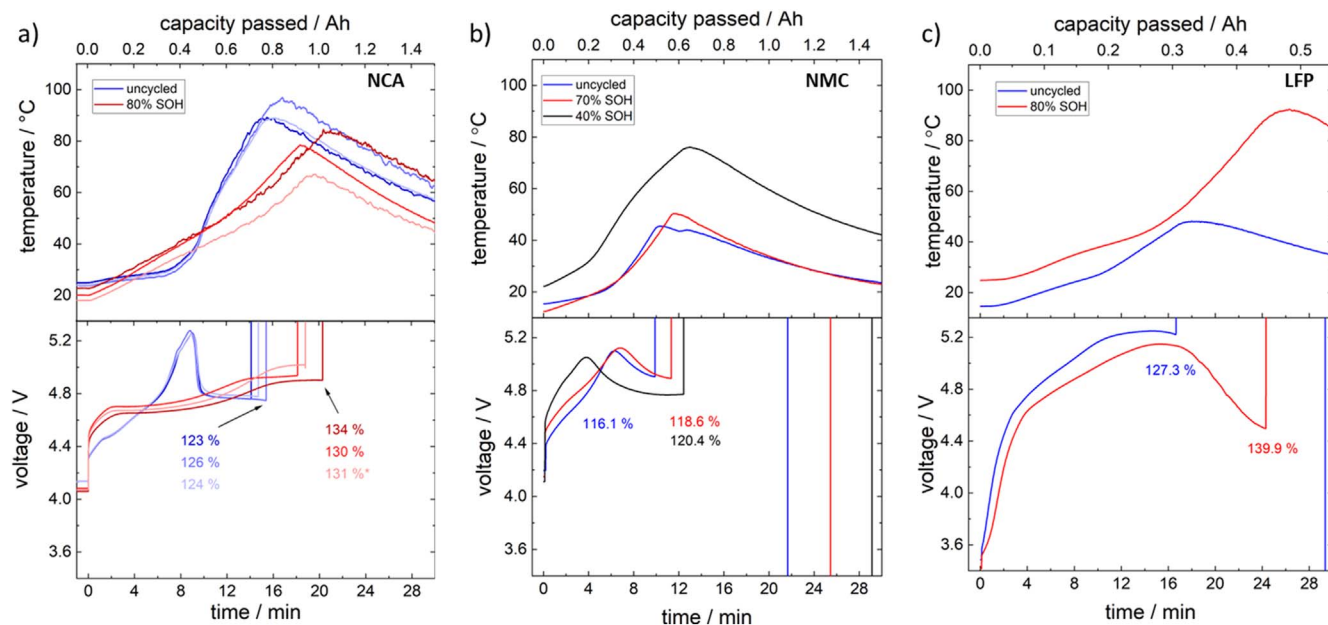
- NCA cells - SOC of CID activation increased from  $124.3 \pm 1.5\%$  (uncycled) to  $139.7 \pm 2.1\%$  (aged–80% SOH)

**Table III. Key setup details for the ARC systems for the different cell types.**

ARC system	Cell mounting	Thermocouple (TC) placement
NCA ES-ARC	Mounted-free hanging in thin steel sheet <sup>a)</sup>	Mid-height of the cylindrical cell surface
LFP ES-ARC	Secured in a metal holder connected to a pressure transducer	Attached to the cell holder using nichrome wire with copper mesh on the TC tip
NMC EV-ARC <sup>b)</sup> (accommodates high energy density cells)	Mounted inside a free-hanging nichrome wire basket	Mid-height of the cell can with copper mesh covering the TC tip

a) Negligible in the ARC data. b) Past tests in the ES- and EV-ARC have shown consistent thermal runaway onset for the same cell.





**Figure 1.** Temperature and voltage behavior during overcharge of (a) NCA, (b) NMC, and (c) LFP cells. Each line corresponds to an experiment with an individual cell. The % values indicate the SOC at CID activation calculated based on the nominal capacity of each cell type.

- NMC cells - SOC of CID activation increased from 116.1% (uncycled) to 118.6% (aged-70% SOH) and 120.4% (aged-40% SOH)

- LFP cells - SOC of CID activation increased from 127.3% (uncycled) to 139.9% (aged-80% SOH)

Previous literature on the timing of CID activation in aged cells relative to fresh cells shows mixed results. Juarez-Robles et al. overcharged 18650 NCA cells with a rate of 1C to 12 V for six hours or failure.<sup>33</sup> For cells aged at 10 °C and 25 °C to 20% capacity fade, CID activation occurred earlier, whereas the cells aged at 40 °C could be overcharged to a similar capacity as fresh cells before CID activation. The authors hypothesized that earlier CID activation in aged cells was due to a build-up of gaseous electrolyte degradation products during aging. Kuntz et al. overcharged 18650 cells with metal oxide positive electrodes with a 1C current up to 8.4 V or failure.<sup>35</sup> Cells cycled for six months or to 20% capacity fade at -20 °C, 0 °C, 25 °C, or 45 °C showed varying behaviors: the two energy cells cycled at 25 °C and 45 °C activated the CID at 1%-2% lower SOC than fresh cells, while a power cell showed CID activation at 1%-2% higher SOC. No materials-based explanation was given for these differences. In contrast, our study found that aged cells consistently required more overcharge time to activate the CID, suggesting that (1) more time is needed to generate sufficient pressure or (2) physical changes in the CID contacts during cycling may require more pressure to break the connection.

We have several hypotheses for why the aged cells in this study may have tolerated more overcharge. One possibility is that LLI in aged cells may diminish the amount of gas produced in the overcharge process. During overcharge, the positive electrode potential increases, which can lead to gas formation and decomposition reactions on its surface.<sup>49</sup> Simultaneously, the anode potential decreases, which can result in Li deposition, even in uncycled cells.<sup>49</sup> However, in aged cells, SEI growth leads to LLI due to reaction of electrolyte and conductive salt on the surface of the graphite particles.<sup>16</sup> LLI during cycling can diminish or prevent Li deposition for aged cells during overcharge and, thus, reduce potential gas generation on the Li surface. Another possibility is that aged cells accepted more overcharge because increased internal resistance caused more overcharge power to dissipate as Joule heating rather than contributing to chemical reactions within the

cell. This would slow down the gas generation required for CID activation. This increased internal resistance is evident in the overall rightward shift of the voltage curves from the uncycled to the aged cells. Additionally, higher  $T_{max}$  values are observed for the aged NMC and LFP cells, although not for the aged NCA cells. Ultimately, further testing is needed to identify the cause of the greater overcharge tolerance of aged cells in this study.

Although the timing of CID activation was consistently later for aged cells, the  $T_{max}$  trends after CID activation varied significantly among chemistries:

- NCA cells -  $T_{max}$  decreased from  $91.7 \pm 4.4$  °C (uncycled cells) to  $76.7 \pm 8.8$  °C (aged cells)

- NMC cells -  $T_{max}$  was consistent between the uncycled cell (50.3 °C) and the 70% SOH cell (47.6 °C), but increased to 76.0 °C for the 40% SOH cell

- LFP cells -  $T_{max}$  increased from 48.1 °C (uncycled cell) to 92.3 °C (aged-80% SOH)

These mixed  $T_{max}$  trends highlight the interplay between chemistry-specific degradation mechanisms, such as cathode reactions and changes in heat dissipation, and the cells' response to overcharge. For all cells,  $T_{max}$  was reached shortly after CID activation, indicating the critical role of internal pressure increase and material decomposition in determining thermal behavior.

We also investigated the cell voltage characteristics before CID activation to understand the electrochemical and material changes occurring in the cells. For uncycled NCA cells, the voltage curves show a peak at ~5.25 V (Fig. 1a), which likely originates from the breakdown of overcharge additives in the electrolyte, such as biphenyl or cyclohexyl benzene, commonly used in commercial applications.<sup>50,51</sup> These additives polymerize during overcharge, forming a protective film on the positive electrode surface while maintaining the voltage at a constant level.<sup>52</sup> However, in the cycled NCA cells, this voltage peak is no longer observed (Fig. 1a), indicating decomposition of the additives during cycle aging at 45 °C prior to the overcharge experiment. For instance, biphenyl has been reported to decompose during aging at similar temperatures in other chemistries.<sup>50</sup> Although electrolyte investigation was beyond the scope of this work, if similar additives were used in the NCA cells, this could explain the differences in voltage profiles for

uncycled and aged cells. In uncycled and aged NMC cells (Fig. 1b), the peak at  $\sim 5.1$  V likely arises from a combination of overcharge reactions and oxygen release from the cathode lattice, which becomes increasingly unstable at high voltages. The voltage rise reflects structural changes in the NMC material as it approaches severe overcharge conditions, with gas generation and electrolyte oxidation contributing to the observed behavior. The uncycled and 70% SOH cells exhibited similar voltage behavior, while the 40% SOH cell showed higher polarization, indicated by a left shift in the peak. This is likely due to an increase in internal resistance in the 40% SOH cell resulting from significant aging. In the case of LFP cells, both uncycled and aged cells exhibit similar voltage profiles up to a peak at 5.1 V and 5.2 V (Fig. 1c), respectively, likely corresponding to electrolyte oxidation and gas generation at the positive electrode. However, the aged cell displayed a significant voltage decrease prior to CID activation, indicating increased internal resistance or reduced ionic conductivity due to aging-related effects such as SEI growth, electrolyte decomposition, or electrode passivation.

Visual failure behavior for the overcharge experiments also varied with chemistry and aging. NCA cells exhibited no venting or weight loss, indicating robust containment in both uncycled and aged states. Overcharge led to venting and smoke in the uncycled NMC cell, while aged NMC cells did not vent, likely due to reduced energy content (Fig. S9–11). For LFP, the uncycled cell exhibited no venting, but the aged cell showed venting and a 0.5 g weight loss, indicating a shift in failure behavior with aging (Fig. S12–13). Additionally, Fig. S7 highlights the results of crush testing conducted after overcharging LFP cells to assess their mechanical stability. The aged cell required greater displacement to trigger TR during crush and once TR was triggered, the  $T_{\max}$  was over 100 °C lower.

Based on the above results and previous literature, it remains challenging to definitively conclude whether aged cells without Li plating are safer or less safe than uncycled cells under overcharge conditions. In this study, aged 18650 cells tolerated a higher overcharge capacity. However, several aged cells (40% aged NMC and 80% aged LFP) showed a higher  $T_{\max}$  than their uncycled counterparts. Lastly, there was minimal difference in ejecta from the uncycled and aged cells, except for the aged LFP cell, which started exhibiting electrolyte leakage. Overall, these results highlight that safety evaluations depend on the specific characteristics considered. It is also important to note that this analysis did not investigate factors such as battery form factor, capacity, and absence of internal safety devices, which can also impact the outcomes of safety tests. For example, previous overcharge experiments of cycle-aged NCA pouch cells without CIDs showed that aged cells with more than 15% capacity fade did not experience TR, unlike fresh cells.<sup>34</sup>

**Overdischarge.**—Overdischarge occurs when a cell is discharged below the manufacturer's recommended lower cut-off voltage (end-of-discharge voltage). This safety hazard is particularly concerning in battery packs where cell capacity imbalance can force weaker cells in series strings into voltage reversal before others complete discharge. Studies of fresh cells indicate that slight overdischarge typically depletes Li inventory from the negative electrode and leads to the decomposition of the SEI.<sup>53</sup> Deeper overdischarge can result in copper dissolution from the negative electrode current collector, initially forming  $\text{Cu}^+$  ions.<sup>43</sup> This dissolution allows copper ions to diffuse/migrate through the electrolyte and deposit as metallic copper or copper compounds on the electrodes.<sup>43</sup> These deposits can block Li intercalation or form copper dendrites upon recharging, which may cause micro-short circuits. The onset cell voltage for copper oxidation varies with cell chemistry, N/P ratio, and overdischarge process.<sup>43</sup> As the onset cell voltage for copper dissolution increases, the risk of copper dissolution and dendrite formation increases; this elevates the possibility of internal short circuits and TR upon recharge. However, overdischarging to 0 V at low C-rates without recharging, as done here, is usually less problematic.<sup>43</sup>

While fresh cells tend to exhibit less severe failures due to overdischarge compared to other abuse modes, there is a notable lack of literature on the effects of overdischarge on aged cells.

Overdischarge abuse testing was conducted on 18650 cells with NCA, NMC, and LFP chemistries in both uncycled and aged states. All cells began at 100% SOC according to the manufacturer's cut-off voltage and were overdischarged at a 1C rate (based on the nominal capacity) until  $-150\%$  SOC or failure. Since the cells were not recharged in the present work, the formation of copper dendrites is not an issue. Figure 2 shows the voltage and temperature profiles for all three chemistries during overdischarge, highlighting critical safety characteristics such as maximum discharge capacity to 0 V (overdischarge tolerance) and  $T_{\max}$ . Visual failure behavior (e.g., electrolyte leakage, venting, fire) was also evaluated.

Overdischarge tolerance was quantified as the capacity discharged between the manufacturer's recommended cut-off voltage (2.5 V for NCA, 2 V for NMC, and 2 V for the LFP cells) and 0 V. The three cell types exhibited varying degrees of overdischarge tolerance prior to dropping to 0 V (reverse potential onset):

- NCA cells (2.5 V to 0 V)—overdischarge tolerance increased from the uncycled cells ( $0.176 \pm 0.005$  Ah) to the aged cells ( $0.403 \pm 0.017$  Ah)
- NMC cells (2 V to 0 V)—overdischarge tolerance decreased slightly from the uncycled cell (0.210 Ah) to the aged cell (0.175 Ah)
- LFP cells (2 V–0 V)—overdischarge tolerance increased from the uncycled cell (0.025 Ah) to the aged cell (0.041 Ah)

The observed values are comparable in magnitude to those previously reported for various LFP, NMC, NCA, and NMC/LMO cells.<sup>43</sup> In general, the aged cells demonstrate greater tolerance to overdischarge conditions, consistent with existing literature.<sup>43</sup> This increased tolerance can be attributed to the rise in internal resistance that typically occurs as cells age, as evidenced by the leftward shift of the voltage curves in Fig. 2. Increased internal resistance causes the cells to reach the 0% SOC voltage limit (manufacturer cut-off) earlier in the normal discharge process. Thus, there is a greater amount of usable capacity within a cell as it is overdischarged to 0 V.

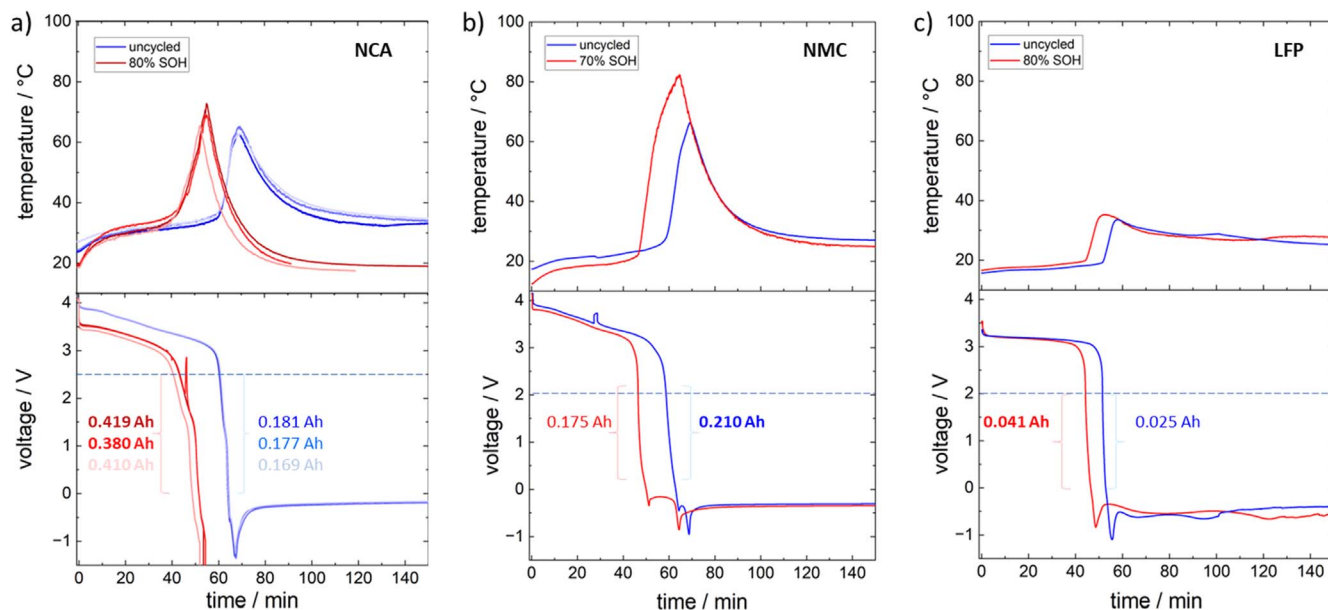
Temperature behavior during overdischarge was largely unaffected by aging in NCA and LFP cells but showed significant changes in NMC cells:

- NCA cells -  $T_{\max}$  increased slightly from the uncycled cells ( $63.6 \pm 1.4$  °C) to the aged cells ( $69.1 \pm 3.6$  °C)
- NMC cells -  $T_{\max}$  increased significantly from the uncycled cell (66.8 °C) to the aged cell (82.9 °C)
- LFP cells -  $T_{\max}$  remained consistent between the uncycled cell (33.9 °C) and the aged cell (34.8 °C)

For each cell,  $T_{\max}$  occurred shortly after the voltage reached 0 V. The increased  $T_{\max}$  in aged NMC cells may reflect greater thermal reactivity due to degradation-induced changes in the electrode materials.

The voltage profiles of aged cells exhibited distinct leftward and downward shifts, indicating increased internal resistance and significant alterations in their electrochemical characteristics due to aging. In aged NCA cells, the absence of the copper dissolution plateau typically observed in uncycled cells is particularly noteworthy. This lack of a plateau suggests that the mechanisms governing copper dissolution have changed.

Beyond the quantitative temperature and voltage data, we also evaluated the visual failure behavior of the overdischarge experiments (Figs. S19–22). For both the NMC and LFP cells, the overdischarge abuse response of the aged cells appeared similar to that of the uncycled cells. None of the cells exhibited CID triggering, cell venting, or weight loss. The uncycled NCA cells also exhibited no venting, but one of the three aged cells vented.



**Figure 2.** Temperature and voltage versus time during overdischarge of (a) NCA, (b) NMC, and (c) LFP cells. Each line corresponds to an experiment with an individual cell. The dashed line on the voltage plot indicates the start of the overdischarge region. The capacity values on the voltage plots indicate the capacity discharged between the manufacturer's recommended cut-off voltage (2.5 V for NCA, 2 V for NMC, and 2 V for the LFP cells) and 0 V.

Based on the above results, aged cells without lithium plating do not have a notably different safety profile from uncycled cells under overdischarge conditions. With the exception of one NMC cell, the aged 18650 cells demonstrated a higher overdischarge capacity tolerance and similar  $T_{\max}$ .

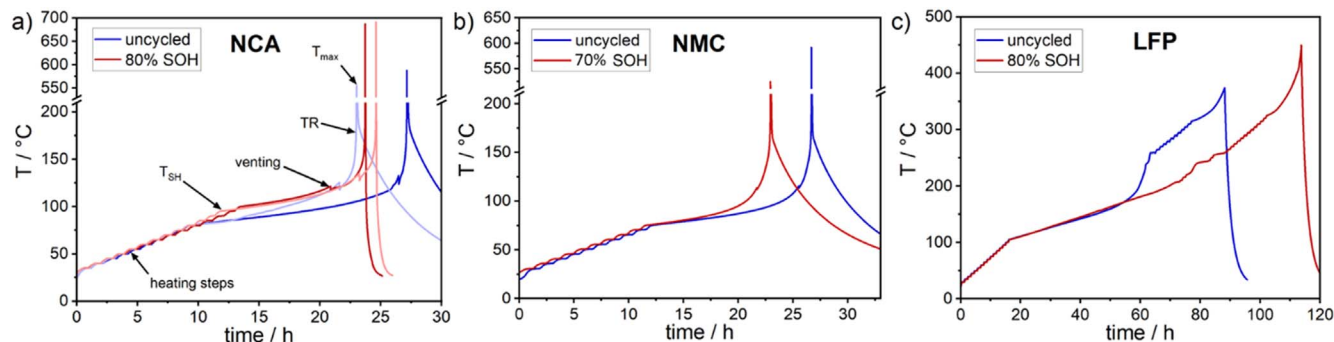
**Accelerating rate calorimetry.**—Batteries in fielded systems can experience thermal abuse when subjected to temperatures exceeding the manufacturer's recommended operating conditions. This situation can arise through inadequate thermal management (whether passive or active), external fires, or malfunctioning electrical components. In laboratory settings, thermal abuse is often investigated through overtemperature tests, where cells are heated at a controlled rate until they reach a set temperature or fail. In this work, we use calorimetry, a form of overtemperature testing that enables precise measurement of a cell's self-heating rate under quasi-adiabatic conditions.

ARC was performed on 18650 cells with NCA, NMC, and LFP chemistries in uncycled and aged conditions. Figure 3 shows the temperature versus time curves from these tests and the characteristic temperatures are listed in Table IV. Critical values include:  $T_{\text{SH}}$  (the onset of self-heating, where the exothermic sensitivity threshold of  $0.02\text{ }^{\circ}\text{C min}^{-1}$  was exceeded for the first time),  $T_{\text{venting}}$  (the temperature of venting),  $T_{\text{TR}}$  (the onset of TR, i.e., a steep increase

in SHR, typically around  $100\text{ }^{\circ}\text{C min}^{-1}$ ),  $T_{\max}$  (the maximum temperature), and SHR (the self-heating rate).

$T_{\text{SH}}$  remained constant or increased for the aged cell of each chemistry, indicating consistent or enhanced safety. The onset of self-heating in uncycled cells is driven by the breakdown of the SEI and typically ranges from  $75$  to  $120\text{ }^{\circ}\text{C}$ , depending on the specific chemistry and cell design.<sup>18,24–26</sup> Knowing the value of  $T_{\text{SH}}$  is critical for effective thermal management, as it indicates the first point of cell degradation due to exothermic reactions. In this study, the  $T_{\text{SH}}$  values for the uncycled cells of the three chemistries were quite different:  $80 \pm 5\text{ }^{\circ}\text{C}$  for the NCA,  $75\text{ }^{\circ}\text{C}$  for the NMC, and  $105\text{ }^{\circ}\text{C}$  for the LFP cells. The  $T_{\text{SH}}$  of the 70% SOH NMC cell and the 80% SOH LFP cell remained unchanged compared to their uncycled counterparts. The NCA cells exhibited a nearly  $20\text{ }^{\circ}\text{C}$  increase in  $T_{\text{SH}}$  for the aged cells (rising from  $80 \pm 5$  to  $98 \pm 5\text{ }^{\circ}\text{C}$ ). This increase aligns with previous literature and is attributed to changes in SEI composition after aging at an elevated temperature of  $45\text{ }^{\circ}\text{C}$ .<sup>24</sup> This behavior is in strong contrast to cells with significant Li plating, where the onset temperature may drop to as low as  $35\text{ }^{\circ}\text{C}$ .<sup>16,25–27,54</sup>

$T_{\text{venting}}$  also remained constant between the uncycled and aged cell of each chemistry. Venting is determined by the abrupt drop in temperature, as indicated in Fig. 3a, due to the cooling effect of the out-streaming gas (Joule-Thomson effect). For NCA,  $T_{\text{venting}}$  was



**Figure 3.** ARC temperature curves of (a) NCA, (b) NMC, and (c) LFP cells. Each line corresponds to an experiment with an individual cell. Characteristic events are marked in (a).

**Table IV.** Characteristic temperatures during ARC testing (in °C) for uncycled and aged cells of different chemistries. If more than one cell was tested, the average is given.

	NCA		NMC		LFP	
	uncycled	80% SOH	uncycled	70% SOH	uncycled	80% SOH
$T_{SH}^a)$	80 ± 5	98 ± 5	75	75	105	105
$T_{venting}^b)$	129 ± 5	128 ± 10	116	114	157.7	156.4
$T_{TR}^c)$	206 ± 1	209 ± 5	204	206	—	—
$T_{max}^d)$	572 ± 23	687 ± 5	591	524	374	450

a) Self-heating onset (ARC exothermic sensitivity threshold exceeds  $0.02\text{ }^{\circ}\text{C min}^{-1}$  for the first time). b) Venting (corresponds to slight temperature decrease). c) Thermal runaway onset (steep increase in SHR, typically around  $100\text{ }^{\circ}\text{C min}^{-1}$ ). d) Maximum temperature.

$129 \pm 5\text{ }^{\circ}\text{C}$  for the uncycled cells and  $128 \pm 10\text{ }^{\circ}\text{C}$  for the aged cells. For NMC,  $T_{venting}$  was  $116\text{ }^{\circ}\text{C}$  for the uncycled cell and  $114\text{ }^{\circ}\text{C}$  for the aged cell. LFP showed higher venting temperatures,  $157.7$  and  $156.4\text{ }^{\circ}\text{C}$  for the uncycled and aged cell, respectively.

The SHR describes the temperature change with time and correlates with the generated heat (assuming constant heat capacity and under adiabatic conditions). This generated heat would have to be dissipated to prevent TR, therefore lower SHR values indicate an increased safety level. Figure 4 illustrates that the overall SHR curves for both NCA and NMC are very similar for uncycled and aged cells, indicating negligible changes due to aging. The uncycled LFP cell demonstrates a higher SHR than its aged counterpart (peaking at  $1\text{ }^{\circ}\text{C min}^{-1}$  rather than  $0.1\text{ }^{\circ}\text{C min}^{-1}$ ), as shown in Fig. 4c. However, the maximum SHR for LFP cells remains significantly lower than that of NCA and NMC cells. The onset of TR ( $T_{TR}$ ) is characterized by a steep increase in the SHR, often at approximately  $100\text{ }^{\circ}\text{C min}^{-1}$ . The NMC and NCA cells exhibit very similar  $T_{TR}$  values for their uncycled and aged cells ( $\sim 205\text{ }^{\circ}\text{C}$ ).

The maximum temperatures during the ARC test, in Table IV, do not show a consistent behavior with aging. While the NCA and LFP cells reached higher values in aged cells, the aged NMC cell had a lower  $T_{max}$  than the uncycled one. Previous literature has shown that aged cells tend to have similar or slightly lower peak temperatures than uncycled cells (likely due to lower energy content).<sup>24</sup>

Overall, the differences between the three different chemistries are more pronounced than the difference between the uncycled and aged cells of any one chemistry. For each chemistry, the onset temperatures for self-heating, venting, and thermal runaway are similar to or slightly elevated for the aged cell. Thus, based on kinetics, the safety profiles of the aged cells are unchanged or slightly safer. It is noteworthy that the NCA and LFP aged cells exhibited higher peak temperatures, however, more data is needed to establish engineering trends.

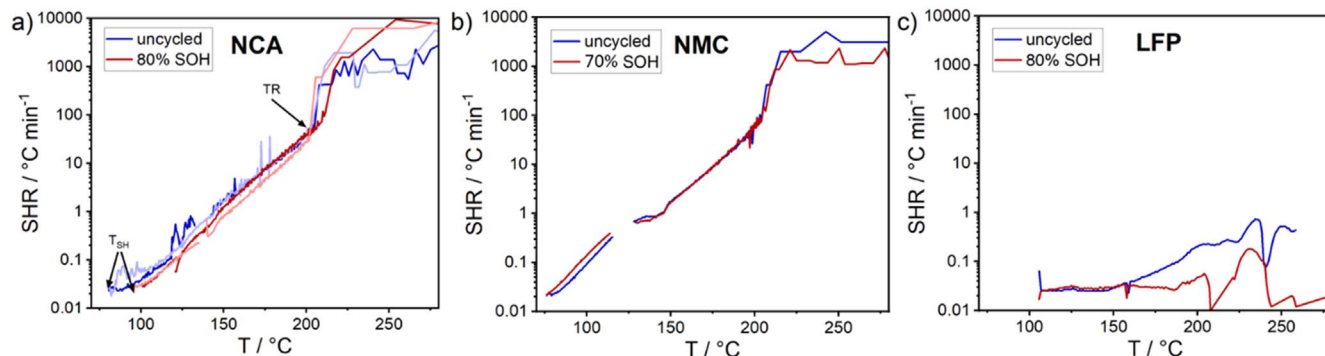
**Nail penetration.**—Nail penetration tests are a valuable tool for assessing the safety behavior of cells under mechanical insult resulting in an internal short circuit (ISC).<sup>55</sup> This safety

consideration is particularly important for batteries used in vehicles, as similar damaging scenarios may arise during traffic accidents.<sup>56</sup> Key safety characteristics assessed during nail penetration include the  $T_{max}$ , displacement (the distance the nail penetrates into the cell), and load (the force exerted on the nail). Lower values of displacement or load indicate that a cell tolerates less abuse prior to entering thermal runaway.

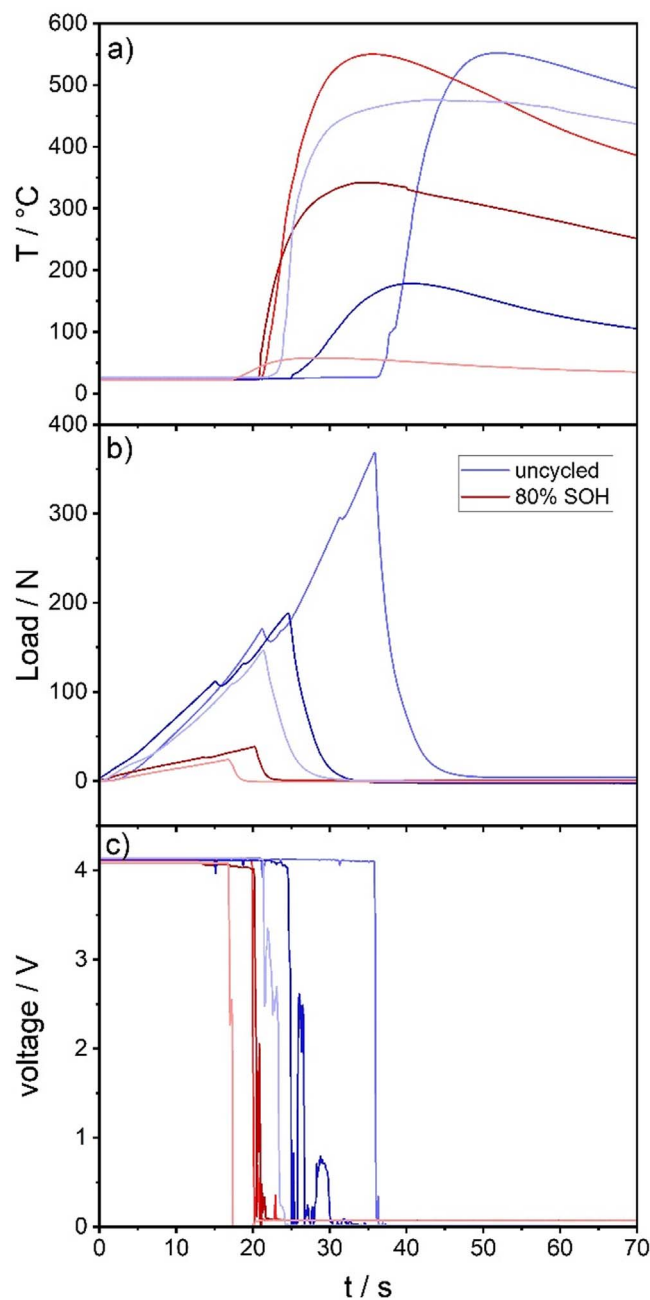
The results of the nail penetration tests for uncycled and  $45\text{ }^{\circ}\text{C}$  aged NCA cells are presented in Fig. 5. The peaks in the load curves (Fig. 5b) mark the points in time after TR was triggered, evident by the significant temperature increases in Fig. 5a. Therefore, the maxima of the load curves mark the penetration of the nail into the cells and the start of creating short circuits.

There is considerable variation in the  $T_{max}$  values measured at the surfaces of the battery cells. The average  $T_{max}$  values at the cell surfaces are  $317 \pm 202\text{ }^{\circ}\text{C}$  for the  $45\text{ }^{\circ}\text{C}$  aged cells and  $402 \pm 161\text{ }^{\circ}\text{C}$  for the uncycled NCA cells. However, when considering the temperatures measured at the positive and negative terminals, the overall  $T_{max}$  values rise to  $423 \pm 112\text{ }^{\circ}\text{C}$  and  $624 \pm 147\text{ }^{\circ}\text{C}$  for the  $45\text{ }^{\circ}\text{C}$  aged and uncycled cells, respectively. In both scenarios, the  $T_{max}$  values for the  $45\text{ }^{\circ}\text{C}$  aged cells are (on average) lower than those for the uncycled cells.

As shown in Fig. 5, the displacement required to trigger TR is slightly lower, indicating reduced safety, in the  $45\text{ }^{\circ}\text{C}$  aged cells ( $2.8 \pm 0.8\text{ mm}$ ) than in the uncycled cells ( $3.2 \pm 0.6\text{ mm}$ ). Previous results on the displacement tolerance of aged cells are mixed. For instance, a study involving the same NCA cells aged to 80% SOH with Li plating also reported a lower displacement value for the aged cells ( $1.9 \pm 0.5\text{ mm}$ ).<sup>31</sup> Conversely, another nail penetration study on 5 Ah LCO-LNCO pouch cells indicated that the displacement required for TR increased as SOH decreased.<sup>57</sup> Additionally, Kovachev et al. observed that greater displacement was needed to trigger TR in 41 Ah NMC-LMO pouch cells (aged at  $60\text{ }^{\circ}\text{C}$ ) compared to their uncycled counterparts.<sup>37</sup> Collectively, these results highlight the importance of cell form factor in abuse response. The mechanical behavior during abuse tests can differ markedly between pouch and cylindrical cells due to variations in the stiffness of the cell housing and the stress induced by the jelly-roll winding.

**Figure 4.** ARC SHR (self-heating rate) curves versus temperature of (a) NCA, (b) NMC, and (c) LFP cells. Onset temperatures of SH and TR are marked in (a). Each line corresponds to an experiment with an individual cell.





**Figure 5.** Nail penetration of NCA cells including the time-dependent (a) temperature measured at the surface of cells, (b) load measured from the nail, and (c) cell voltage. Each line corresponds to a different cell. There is a linear correlation between time and displacement of the nail.

In Fig. 5b, the maximum measured load ( $F_{\max}$ ) is significantly lower in the 45 °C aged cells ( $31 \pm 7$  N) than in the uncycled cells ( $235 \pm 96$  N). Notably, all of the uncycled cells and one of the 45 °C aged cells show small drops in load that correspond with decreases in cell voltage, indicating the presence of soft shorts.<sup>55,58,59</sup> Since a ceramic nail was used in this study, all shorts are induced by the mechanical deformation and electrical contact of the cell materials rather than by the nails themselves. Other studies have reported peaks in load measurements and attributed them to the piercing of the cell housing and electrode layers.<sup>60,61</sup>

Various studies have shown that electrode thickness increases during aging, increasing the internal mechanical pressure within cells that have a rigid housing.<sup>62–66</sup> The post-mortem analysis of the aged NCA cells, where SEI growth was identified as the primary

aging mechanism, revealed a 10% increase in the thickness of the negative electrode compared to uncycled cells.<sup>31</sup> This suggests that the aged cells likely exhibit an increase in internal pressure. The higher pressure applied to the inside of the cell casing increases its rigidity, potentially making it easier to puncture at lower applied forces (and have earlier onset of TR), as shown in Fig. 5.

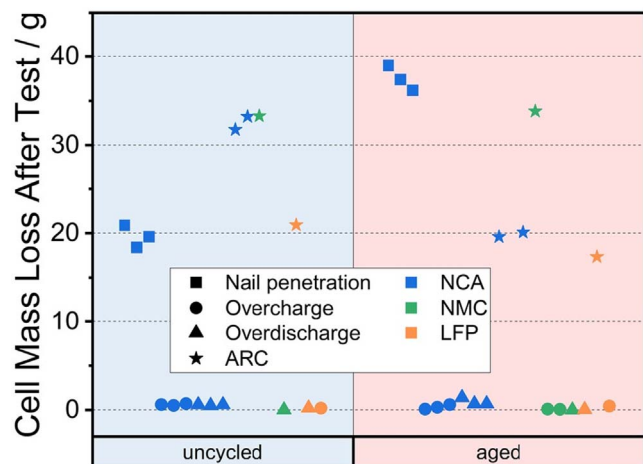
Based on the results presented here and available literature data, the relative safety of aged cells without Li plating during nail penetration varies depending on the form factor and the safety characteristic. The state of safety of a cell encompasses different characteristics and a cell can be deemed less safe in one characteristic and more safe in another. Aged NCA cells with SEI growth required less mechanical abuse (indicated by lower displacement and  $F_{\max}$ ) to trigger TR compared to uncycled cells. In contrast, pouch cells in previous studies required a higher displacement to trigger TR, showing that the impact of form factor merits further investigation.<sup>37,57</sup> Once TR was triggered, the aged cells in this study showed, on average, a lower  $T_{\max}$  than the uncycled cells. However, it is challenging to comment on differences in the severity of TR given the lack of consistency in peak temperature across the replicates. Such variability is more common for nail penetration than other abuse tests.

**Overall evaluation.**—In addition to assessing characteristics specific to individual battery safety tests (such as time to overcharge and mechanical displacement), we also considered characteristics that are common across all tests. Evaluating the different abuse techniques in relation to one another is crucial, as it highlights the areas where battery aging has the most pronounced effect. The characteristics analyzed across all tests include mass loss, maximum temperature, and EUCAR hazard level.<sup>67</sup>

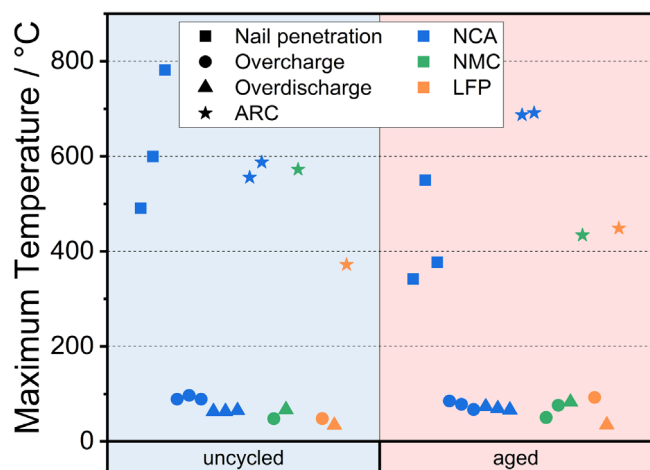
Measuring mass loss provides valuable insight into the extent of cell destruction and serves as a straightforward method for assessing the intensity of TR. Additionally, considering mass loss is important because ejecta from a single cell can contribute to propagation of thermal runaway within a battery system. As illustrated in Fig. 6, there are significant variations in mass loss across different safety testing methods. In this study, the influence of cell chemistry and aging state was less significant than the impact of the safety test method itself. Overcharge and overdischarge tests show consistently negligible mass loss across all cell chemistries, regardless of whether the cells were uncycled or aged. Uncycled NCA cells show a loss of about 40% of their initial mass after nail penetration tests. However, the 45 °C aged NCA cells subject to nail penetration show the highest mass loss (77% of the starting mass) among all tests conducted in this study, with only the can remaining intact. This significant mass loss indicates a strong TR behavior, correlated with an explosion of the cell.

Cells subjected to ARC testing consistently exhibited significant mass loss, with variation depending on the cell chemistry and aging condition. For NCA, uncycled cells showed greater mass loss (~66% with respect to the starting mass) than aged cells (~44%). This difference is visually apparent when comparing the physical state of the cells after the test. In uncycled NCA cells, the cap was completely detached, whereas in aged NCA cells, the cap remained attached to the can. However, the jelly roll was ejected in both cases, likely in a pulverized form, escaping through the venting holes in the aged cell. By contrast, the NMC and LFP cells exhibited consistent mass loss in the ARC in the uncycled and aged state. For NMC and LFP, the jelly roll partially ejected from the can during thermal runaway for both uncycled and aged cells.

The maximum temperature serves as an indicator of the severity of the TR and the associated heat release (Fig. 7). In overcharge and overdischarge experiments, the thermal behavior was relatively mild, with  $T_{\max}$  rarely exceeding 100 °C for both uncycled and aged cells across all chemistries. Nail penetration tests on NCA cells, on the other hand, resulted in more severe TR.  $T_{\max}$  for the uncycled cells was on average 200 °C higher than the aged cells. This may be attributed to the greater mass loss from the aged cells as this removes



**Figure 6.** Comparison of cell mass loss after test for different cell chemistries and safety tests on uncycled and aged cells (without Li plating).

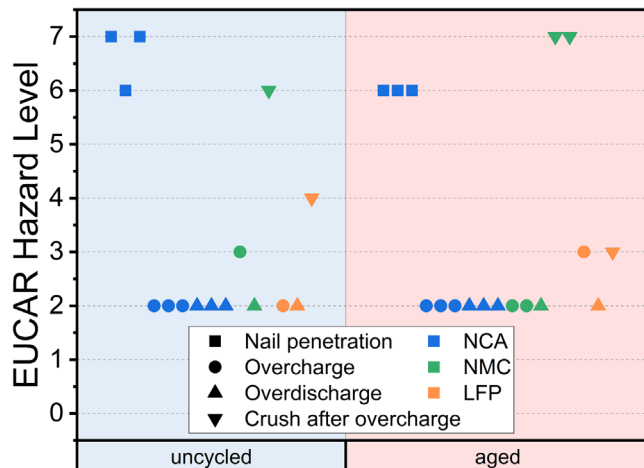


**Figure 7.** Comparison of maximum temperature during safety testing with different methods on uncycled and aged cells without Li plating.

hot material from the cell. ARC experiments showed similarly elevated temperatures as nail penetration tests, but no clear trend was observed between uncycled and aged cells. Aged NCA and LFP cells had a  $T_{\max}$  nearly 100 °C higher than their uncycled counterparts, whereas the  $T_{\max}$  of the aged NMC cell was about 70 °C lower than that of the uncycled cell.

Finally, EUCAR Hazard Severity Levels (HSLs) were assigned to provide a standardized numerical assessment of the safety of each cell (Fig. 8).<sup>67</sup> It is important to note that the evaluation of the EUCAR HSLs in this study pertains specifically to the 18650 cells discussed. The HSL evaluation was based on recorded videos of the safety tests. Since no videos were available for the ARC tests, no HSL evaluation was conducted for this type of safety test.

In the overcharge and overdischarge tests, most cells received an HSL of 2, except for uncycled NMC cells and an aged LFP cell, which were assigned an HSL of 3 (Figs. S9–13 and S19–22). An HSL of 2 was assigned based on CID activation and the resulting loss of cell functionality (no charge and/or no voltage). Cells assigned an HSL of 3 displayed electrolyte leakage and light smoke. Importantly, none of these cells experienced TR or catastrophic disruption. Aging improved the safety of NMC cells during overcharge (no electrolyte leakage), while it decreased the safety of the LFP cell (Figs. S12–13). These findings are consistent with the mass loss and maximum temperature evaluations.



**Figure 8.** Comparison of the EUCAR hazard level for safety testing with different methods on uncycled and aged cells without Li plating.

Crush tests conducted after overcharge revealed very high HSLs of 7 for both uncycled and aged NMC cells (Figs. S14–16). During the initial overcharge test, the cells were charged until the CID activated, which electrically isolated the cell in the overcharged state. Therefore, the HSL of the crush test on the overcharged cells demonstrated more significant effects during failure. The overcharged cells subjected to crush tests exhibited energetic venting during initial rupture, accompanied by fire, flames, and gas generation. In contrast, crush tests following overcharge of LFP cells resulted in cell rupture, venting, and the production of heavy smoke (HSL of 4, Fig. S17). For the aged LFP cell, the HSL decreased to 3 as it only exhibited light smoke, electrolyte leakage, and no signs of rupture (Fig. S18).

Nail penetration tests on uncycled NCA cells resulted in severe TR with an HSL of 7. Cell explosions resulted in total disintegration and the ejection of numerous burning particles. The TR reactions in the aged NCA cells were slightly less severe (HSL of 6), even though they exhibited twice the mass loss.

### Impact of Aging Method

In our previous study with the NCA cells used here, we explored the effect of a different aging mechanism, Li plating, on safety performance.<sup>31</sup> Post-mortem analysis and electrochemical experiments confirmed Li plating as the main aging mechanism for those NCA cells (cycle-aged at 0 °C) and SEI growth as the main aging mechanism for the cells used in this study (cycle-aged at 45 °C). In this section, we compare the relative changes in safety characteristics—for overcharge, overdischarge, ARC, and nail penetration—for the two different aging mechanisms.

During **overcharge**, aged cells with Li plating consistently exhibited a more severe response than uncycled cells and aged cells with SEI growth.<sup>31</sup> Both cells with Li plating<sup>31</sup> and SEI growth showed a later CID triggering than the uncycled cells. However, overcharged NCA cells with Li plating showed higher  $T_{\max}$  than uncycled cells, whereas overcharged cells with SEI growth showed lower  $T_{\max}$ . The increase in  $T_{\max}$  for cells with Li plating can be attributed to the exothermic reaction between the Li metal and the electrolyte, as shown in experiments<sup>25,68</sup> and *ab initio* molecular dynamics simulations.<sup>69</sup> While uncycled NCA cells and those with SEI growth maintained EUCAR HSLs of 2, the HSLs of cells with Li plating increased significantly, ranging from 2 to 6.<sup>31</sup> In **overdischarge** tests, both the cycled NCA cells with Li plating<sup>31</sup> and those with SEI growth showed behavior similar to that of uncycled cells, with all assigned EUCAR HSLs of 2.

In **ARC** experiments, Li plating adversely affected the safety profile. Cycled NCA cells with SEI growth had values similar to that

of uncycled cells for SHR as a function of temperature,  $T_{\text{vent}}$ , and  $T_{\text{TR}}$ . Cells with SEI growth even showed a delayed  $T_{\text{SH}}$  (increasing from  $80 \pm 5$  °C in the uncycled cells to  $98 \pm 5$  °C in the aged cells with SEI growth). In contrast, when the dominant aging mechanism was Li plating,  $T_{\text{SH}}$  dropped to  $35 \pm 5$  °C.<sup>31</sup> This decrease is consistent with previous literature<sup>24</sup> and highlights how thermal runaway can accidentally be initiated in cells with Li plating under conditions not typically considered abusive.

Finally, in **nail penetration** tests, the EUCAR HSLs were consistently high (6–7) across all NCA cells, regardless of whether they were uncycled or exhibited Li plating<sup>31</sup> or SEI growth as the dominant aging mechanism. Aged NCA cells with either Li plating<sup>31</sup> or SEI growth required less mechanical abuse (indicated by lower displacement and  $F_{\text{max}}$ ) to initiate TR compared with the uncycled cells. However, once TR was initiated, the average  $T_{\text{max}}$  was slightly higher for the NCA cells with Li plating<sup>31</sup> than uncycled cells, while those with SEI growth had slightly lower temperatures.

In summary, the impact of the aging mechanism on the severity of the TR response depends on the safety test conducted. Aged NCA cells with Li plating exhibited significantly more severe failures than uncycled cells and cells with SEI growth when subject to overcharge and ARC. However, all NCA cells exhibited a similar response severity for overdischarge and nail penetration. Critically, aging, regardless of the mechanism, altered the sensitivity to TR triggering compared to uncycled cells. For both SEI growth and Li plating, failure was triggered earlier during nail penetration compared to the uncycled cells and later during overcharge and overdischarge.

## Conclusions

The evaluation of safety in aged lithium-ion batteries is a relatively unexplored area, but it has become increasingly important as batteries are used for longer periods. In this study, we investigated the abuse response of commercial 18650 cells, with NCA, NMC, and LFP positive electrodes, aged under conditions that promoted SEI growth rather than Li plating. We compared their response against uncycled cells during overcharge, overdischarge, ARC, and nail penetration tests.

Overall, the uncycled and aged cells exhibited a similar magnitude of TR in response to abuse. However, in some cases, the sensitivity to triggering TR changed. Key findings from the abuse tests in this study include:

- **Overcharge:** All aged 18650 cells tolerated a higher overcharge capacity prior to CID activation. However, several aged cells (40% remaining capacity NMC and 80% LFP) showed a higher  $T_{\text{max}}$  than their uncycled counterparts.
- **Overdischarge:** With the exception of the NMC cell, the aged 18650 cells demonstrated a higher tolerance for overdischarge and lower  $T_{\text{max}}$  values.
- **ARC:** In line with previous literature on the thermal abuse of aged cells without Li plating, the onset temperatures for thermal events were consistent between uncycled and aged cells. However, the  $T_{\text{max}}$  was higher for aged NCA and LFP cells.
- **Nail penetration:** Aged NCA cells with SEI growth required less mechanical abuse (indicated by lower displacement and  $F_{\text{max}}$ ) to trigger TR compared to uncycled cells. However, once TR commenced, the average  $T_{\text{max}}$  for the aged cells was lower.
- **Crush after overcharge:** Aged cells showed lower  $T_{\text{max}}$  values.
- **EUCAR:** The EUCAR levels for all aged cells were equal to or lower than those of their uncycled counterparts. The exception was an aged LFP cell, which, in contrast to the uncycled cell, experienced electrolyte leakage during overcharge.



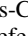
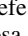
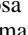


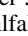

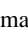
Our previous assessment of NCA cells with the main aging mechanism of Li plating showed that aged cells were less safe across more safety characteristics.<sup>31</sup> This highlights the necessity of evaluating the safety of aged batteries across diverse degradation modes. Additional factors that may have a substantial impact on the

safety assessment of aged cells, and should be studied further, include form factor, capacity/energy content, and module configuration. Understanding the differences between aged and uncycled batteries is vital for developing more effective failure mitigation strategies, particularly as batteries are increasingly considered for second-life applications.

## Acknowledgments

The safety tests on NMC/LFP and NCA cells were conducted at Sandia National Labs and at ZSW, respectively. We thank Dr. Joshua Lamb for providing critical feedback on the manuscript. This material is based upon work supported by the U.S. Department of Energy, Office of Electricity (OE), Energy Storage Division. This article has been authored by an employee of National Technology & Engineering Solutions of Sandia, LLC under Contract No. DE-NA0003525 with the U.S. Department of Energy (DOE). The employee owns all right, title and interest in and to the article and is solely responsible for its contents. The United States Government retains and the publisher, by accepting the article for publication, acknowledges that the United States Government retains a non-exclusive, paid-up, irrevocable, world-wide license to publish or reproduce the published form of this article or allow others to do so, for United States Government purposes. The DOE will provide public access to these results of federally sponsored research in accordance with the DOE Public Access Plan <https://www.energy.gov/downloads/doe-public-access-plan>. ZSW acknowledges funding of the projects CIRCULUS (03ETE035F) by the German Federal Ministry of Economic Affairs and Climate Action (BMWK) and AnaLiBa (03XP0347C) within the AQua-Cluster and HighSafe-III (03XP0568C) by the German Federal Ministry of Education and Research (BMBF).

## ORCID

Yuliya Preger  <https://orcid.org/0000-0001-8558-2529>  
 Max Feinauer  <https://orcid.org/0000-0003-2483-8257>  
 Loraine Torres-Castro  <https://orcid.org/0000-0002-9267-8489>  
 Christine Hogrefe  <https://orcid.org/0000-0001-9952-8507>  
 Gabriela Gerosa  <https://orcid.org/0000-0001-8701-965X>  
 Reed M. Wittman  <https://orcid.org/0000-0003-1529-0517>  
 Markus Hölzle  <https://orcid.org/0009-0004-8278-1089>  
 Nathan Brenner Johnson  <https://orcid.org/0000-0002-1360-110X>  
 Margret Wohlfahrt-Mehrens  <https://orcid.org/0000-0002-5118-5215>  
 Thomas Waldmann  <https://orcid.org/0000-0003-3761-1668>

## References

1. D. H. Doughty and E. P. Roth, *The Electrochemical Society Interface*, **21**, 37 (2012).
2. P. Jindal and J. Bhattacharya, *J. Electrochem. Soc.*, **166**, A2165 (2019).
3. Q. Wang, B. Mao, S. I. Stoliarov, and J. Sun, *Prog. Energy Combust. Sci.*, **73**, 95 (2019).
4. L. Bravo Diaz, X. He, Z. Hu, F. Restuccia, M. Marinescu, J. V. Barreras, Y. Patel, G. Offer, and G. Rein, *J. Electrochem. Soc.*, **167**, 090559 (2020).
5. Z. Liao, S. Zhang, K. Li, G. Zhang, and T. G. Habetler, *J. Power Sources*, **436**, 226879 (2019).
6. T. Cai, A. G. Stefanopoulou, and J. B. Siegel, *ECS Trans.*, **89**, 85 (2019).
7. L. Torres-Castro, A. M. Bates, N. B. Johnson, G. Quintana, and L. Gray, *J. Electrochem. Soc.*, **171**, 020520 (2024).
8. M. Feinauer, A. A. Abd-El-Latif, P. Sichter, A. Aracil Regalado, M. Wohlfahrt-Mehrens, and T. Waldmann, *J. Power Sources*, **570**, 233046 (2023).
9. T. Joshi, S. Azam, C. Lopez, S. Kinyon, and J. Jeevarajan, *J. Electrochem. Soc.*, **167**, 140547 (2020).
10. J. Lamb, L. Torres-Castro, J. C. Hewson, R. C. Shurtz, and Y. Preger, *J. Electrochem. Soc.*, **168**, 060516 (2021).
11. C. R. Birkl, M. R. Roberts, E. McTurk, P. G. Bruce, and D. A. Howey, *J. Power Sources*, **341**, 373 (2017).
12. M. R. Palacin, *Chem. Soc. Rev.*, **47**, 4924 (2018).
13. T. Waldmann, B.-I. Hogg, and M. Wohlfahrt-Mehrens, *J. Power Sources*, **384**, 107 (2018).
14. M. Dubarry, C. Truchot, B. Y. Liaw, K. Gering, S. Sazhin, D. Jamison, and C. Michelbacher, *J. Power Sources*, **196**, 10336 (2011).
15. D. Anseán, G. Baure, M. González, I. Cameán, A. B. García, and M. Dubarry, *J. Power Sources*, **459**, 227882 (2020).

16. M. Feinauer, A. A. Abd-El-Latif, P. Sichler, M. Wohlfahrt-Mehrens, M. Hölzle, and T. Waldmann, *J. Electrochem. Soc.*, **171**, 110524 (2024).
17. X. Feng, D. Ren, S. Zhang, X. He, L. Wang, and M. Ouyang, *Int. J. Electrochem. Sci.*, **14**, 44 (2019).
18. B. Timke, M. Winter, and P. Niehoff, *J. Electrochem. Soc.*, **171**, 070538 (2024).
19. L. Zhang, L. Liu, A. Terekhov, D. Warnberg, and P. Zhao, *Process Safety and Environmental Protection*, **185**, 910 (2024).
20. V. Kabra, A. Karmakar, B. S. Vishnugopi, and P. P. Mukherjee, *Energy Storage Mater.*, **74**, 103878 (2025).
21. M. Börner, A. Friesen, M. Grütze, Y. P. Stenzel, G. Brunklaus, J. Haetge, S. Nowak, F. M. Schappacher, and M. Winter, *J. Power Sources*, **342**, 382 (2017).
22. Z. Cai, S. Mendoza, J. Goodman, J. McGann, B. Han, H. Sanchez, and R. Spray, *J. Electrochem. Soc.*, **167**, 160515 (2020).
23. F. Larsson, S. Bertilsson, M. Furlani, I. Albinsson, and B.-E. Mellander, *J. Power Sources*, **373**, 220 (2018).
24. Y. Preger, L. Torres-Castro, T. Rauhala, and J. Jeevarajan, *J. Electrochem. Soc.*, **169**, 030507 (2022).
25. M. Fleischhammer, T. Waldmann, G. Bisle, B.-I. Hogg, and M. Wohlfahrt-Mehrens, *J. Power Sources*, **274**, 432 (2015).
26. T. Waldmann, J. B. Quinn, K. Richter, M. Kasper, A. Tost, A. Klein, and M. Wohlfahrt-Mehrens, *J. Electrochem. Soc.*, **164**, A3154 (2017).
27. T. Waldmann and M. Wohlfahrt-Mehrens, *Electrochim. Acta*, **230**, 454 (2017).
28. A. Friesen, F. Horsthemke, X. Mönnighoff, G. Brunklaus, R. Krafft, M. Börner, T. Risthaus, M. Winter, and F. M. Schappacher, *J. Power Sources*, **334**, 1 (2016).
29. H. Zhou, A. S. Alujage, M. Terese, C. Fear, T. Joshi, V. R. Rikka, J. A. Jeevarajan, and P. P. Mukherjee, *Chem. Eng. J.*, **492**, 152181 (2024).
30. H. Zhou, A. S. Alujage, M. Terese, C. Fear, T. Joshi, V. R. Rikka, J. A. Jeevarajan, and P. P. Mukherjee, *Appl. Energy*, **377**, 124465 (2025).
31. G. G. Gerosa, M. Feinauer, C. Hogrefe, S. Häfele, K. Bischof, M. Wörz, O. Böse, M. Wohlfahrt-Mehrens, M. Hölzle, and T. Waldmann, *J. Electrochem. Soc.*, **172**, 030502 (2024).
32. L. Feng, L. Jiang, J. Liu, Z. Wang, Z. Wei, and Q. Wang, *J. Power Sources*, **507**, 230262 (2021).
33. D. Juarez-Robles, S. Azam, J. A. Jeevarajan, and P. P. Mukherjee, *J. Electrochem. Soc.*, **168**, 050535 (2021).
34. D. Juarez-Robles, S. Azam, J. A. Jeevarajan, and P. P. Mukherjee, *J. Electrochem. Soc.*, **168**, 110501 (2021).
35. P. Kuntz, L. Lonardonì, S. Genies, O. Raccourt, and P. Azaïs, *Batteries*, **9**, 427 (2023).
36. S. Hildebrand, A. Friesen, J. Haetge, V. Meier, F. Schappacher, and M. Winter, *ECS Trans.*, **74**, 85 (2016).
37. G. Kovachev, C. Ellersdorfer, G. Gstrein, I. Hanzu, H. M. R. Wilkening, T. Werling, F. Schauwecker, and W. Sinz, *eTransportation*, **6**, 100087 (2020).
38. Y. Liu, Y. Xia, and Q. Zhou, *Energy Storage Mater.*, **40**, 268 (2021).
39. Y. Jia, X. Gao, L. Ma, and J. Xu, *Adv. Energy Mater.*, **13**, 2300368 (2023).
40. C. Wang and Y. Xia, *J. Electrochem. Soc.*, **170**, 060543 (2023).
41. E. Micheli, C. Ellersdorfer, I. Hanzu, G. Hofer, P. Höschle, and J. Moser, *J. Power Sources*, **611**, 234768 (2024).
42. Y. Qu, B. Xing, Y. Xia, and Q. Zhou, *eTransportation*, **20**, 100331 (2024).
43. M. Flügel, M. Kasper, C. Pfeifer, M. Wohlfahrt-Mehrens, and T. Waldmann, *J. Electrochem. Soc.*, **168**, 020506 (2021).
44. Y. Preger, H. M. Barkholtz, A. Fresquez, D. L. Campbell, B. W. Juba, J. Romàn-Kustas, S. R. Ferreira, and B. Chalamala, *J. Electrochem. Soc.*, **167**, 120532 (2020).
45. R. Wittman et al., *J. Electrochem. Soc.*, **170**, 120538 (2023).
46. Z. Dobó, T. Dinh, and T. Kulcsár, *Energy Reports*, **9**, 6362 (2023).
47. T. Ohsaki, T. Kishi, T. Kuboki, N. Takami, N. Shimura, Y. Sato, M. Sekino, and A. Satoh, *J. Power Sources*, **146**, 97 (2005).
48. Q. Yuan, F. Zhao, W. Wang, Y. Zhao, Z. Liang, and D. Yan, *Electrochim. Acta*, **178**, 682 (2015).
49. M. Wohlfahrt-Mehrens and T. Waldmann, "Lithium batteries - Secondary systems —Lithium-ion systems | Aging mechanisms and lifetime predictions." *Encyclopedia of Electrochemical Power Sources* (Elsevier, Germany) 412 (2024).
50. B. P. Matadi et al., *J. Electrochem. Soc.*, **164**, A1089 (2017).
51. Y. Chen, *Ionics*, **28**, 495 (2022).
52. Y. Luo, C. Sang, K. Le, H. Chen, H. Li, and X. Ai, *Journal of Energy Chemistry*, **94**, 181 (2024).
53. D. Juarez-Robles, A. A. Vyas, C. Fear, J. A. Jeevarajan, and P. P. Mukherjee, *J. Electrochem. Soc.*, **167**, 090558 (2020).
54. A. A. Abd-El-Latif, P. Sichler, M. Kasper, T. Waldmann, and M. Wohlfahrt-Mehrens, *Batteries & Supercaps*, **4**, 1135 (2021).
55. J. Lamb and C. J. Orendorff, *J. Power Sources*, **247**, 189 (2014).
56. P. Sun, R. Bisschop, H. Niu, and X. Huang, *Fire Technol.*, **56**, 1361 (2020).
57. S. Doose, A. Hahn, S. Fischer, J. Müller, W. Haselrieder, and A. Kwade, *Journal of Energy Storage*, **62**, 106837 (2023).
58. B. Liu, Y. Jia, C. Yuan, L. Wang, X. Gao, S. Yin, and J. Xu, *Energy Storage Mater.*, **24**, 85 (2020).
59. N. Böttcher, S. Dayani, H. Markötter, A. Bau, M. Setzchen, A. Schmidt, J. Kowal, and J. Krug von Nidda, *Energy Technology*, **12**, 2301379 (2024).
60. T. Ma, L. Chen, S. Liu, Z. Zhang, S. Xiao, B. Fan, L. Liu, C. Lin, S. Ren, and F. Wang, *J. Power Sources*, **437**, 226928 (2019).
61. L. Zhang, Y. Liu, and X. Huang, *Int. J. Heat Mass Transfer*, **233**, 126020 (2024).
62. M. Petzl, M. Kasper, and M. A. Danzer, *J. Power Sources*, **275**, 799 (2015).
63. J. Sturm, F. B. Spingler, B. Rieger, A. Rheinfeld, and A. Jossen, *J. Electrochem. Soc.*, **164**, A1342 (2017).
64. R. Li, D. Ren, D. Guo, C. Xu, X. Fan, Z. Hou, L. Lu, X. Feng, X. Han, and M. Ouyang, *J. Electrochem. Soc.*, **166**, A4106 (2019).
65. V. Müller, R.-G. Scurtu, K. Richter, T. Waldmann, M. Memm, M. A. Danzer, and M. Wohlfahrt-Mehrens, *J. Electrochem. Soc.*, **166**, A3796 (2019).
66. R. Li, W. Li, A. Singh, D. Ren, Z. Hou, and M. Ouyang, *Energy Storage Mater.*, **52**, 395 (2022).
67. European Council for Automotive R&D, *Battery Requirements for Future Automotive Applications* (EUCAR) (2019).
68. H. Kondou, J. Kim, and H. Watanabe, *Electrochemistry*, **85**, 647 (2017).
69. D. Stottmeister and A. Groß, *Batteries & Supercaps*, **6**, e202300156 (2023).